Soft Matter

ROYAL SOCIETY OF CHEMISTRY

PAPER

View Article Online
View Journal | View Issue

Cite this: *Soft Matter*, 2021, **17**, 145

Chlamydomonas reinhardtii swimming in the Plateau borders of 2D foams†

Oskar Tainio, [a] Fereshteh Sohrabi, [a] Nikodem Janarek, [ab] Juha Koivisto, *[a] Antti Puisto, [a] Leevi Viitanen, [a] Jaakko V. I. Timonen [a] and Mikko Alava [a]

Received 1st July 2020,
Accepted 8th October 2020

DOI: 10.1039/d0sm01206h

rsc.li/soft-matter-journal

Unicellular *Chlamydomonas reinhardtii* micro-algae cells were inserted into a quasi-2D Hele-Shaw chamber filled with saponin foam. The movement of the algae along the bubble borders was then manipulated and tracked. These self-propelled particles generate flow and stresses in their surrounding matter. In addition, the algae possess the capability of exerting forces that alter bubble boundaries while maintaining an imminent phototactic movement. We find that by controlling the gas fraction of the foam we can change the interaction of the algae and bubbles. Specifically, our data expose three distinct swimming regimes for the algae with respect to the level of confinement due to the Plateau border cross-section: unlimited bulk, transition, and overdamped regimes. At the transition regime we find the speed of the algae to be modeled by a simple force balance equation emerging from the shear inside the Plateau border. Thus, we have shown that it is possible to create an algae-friendly foam while controlling the algae motion. This opens doors to multiple applications where the flow of nutrients, oxygen and recirculation of living organisms is essential.

1 Introduction

Novel biomaterials have recently attracted a lot of attention. New functions of bio-based materials are being actively researched through, for instance, foam based processing allowing the manufacturing of lightweight materials. The dynamics of self-propelled particle systems is another active field of research with recent advances in particles moving in structured or periodic potentials.[1] In Fig. 1 and in the ESI,† we show an example of a combination of the two systems, a 2D foam and living algae particles swimming between the bubbles. The typical experimental setup is a 2D Hele-Shaw cell.[2] In additions to foams, these devices have been noted to be efficient for monitoring the motion of microswimmers.[3,4]

Foams are structures composed of bubbles separated by liquid films. The bubbles are stabilized by reducing the gas–liquid interface tension using appropriate surface active materials. In addition to the gas fraction, foam phase compositions and rheological properties are defined by surfactants, polymers, and the applied shear rate $\dot{\gamma}$.[5] However, many commonly used surfactants are antimicrobial killing living organisms. This makes the preparation of a bio-compatible foam a challenging task. Nevertheless, thanks to their large available surface area, bio-compatible foams offer a promising route to novel photo-bioreactors potentially enabling higher biomass densities compared to other cultivation methods.[6]

The hydrodynamics of micro-organisms differs from beings of macroscopic size by the dependencies on the surrounding inertial and viscous forces present in the liquid.[7] The motility is altered by the flow field, characterized by the Reynolds number.

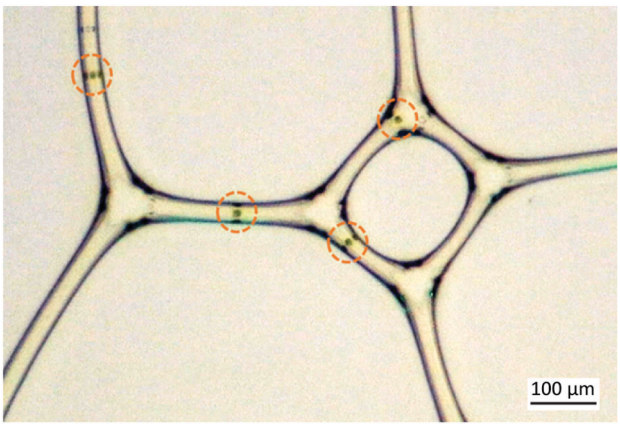

Fig. 1 2D foam creates channels for the green algae particles swimming in it. The dark lines are the fluid–air interface separating the large nearly polygonal bubbles from rod-like films. The movement of the algae can be manipulated by the green light outside the frame attracting the algae towards the lower left corner. The algae are highlighted by dashed circles.

[a] *Department of Applied Physics, Aalto University, 00076 Aalto, Finland. E-mail: juha.koivisto@aalto.fi*
[b] *Department of Physics and Astronomy, University College London, UK*

† Electronic supplementary information (ESI) available: Video of Fig. 1 is available at https://youtu.be/7JGyHUgxPz0. See DOI: 10.1039/d0sm01206h

When the Reynolds number is low, the algae cell is able to alter its swimming direction from the local, intrinsic flow of the liquid. In this case, the algae cell swims according to the scallop theorem proposed by Purcell.[8]

The ability of living organisms to perform tasks such as searching for food or light, or spreading off-spring is largely enabled by their capability of locomotion.[9] Instead of swimming around randomly, many micro-organisms optimize their process by establishing their direction of motion on gradients in chemical,[10] viscous,[11,12] or lighting environments.[13] This is called *taxis*. The particular type of algae discussed here, the *Chlamydomonas reinhardtii* (*C. reinhardtii*), is phototactic.[14,15] Therefore, once successfully maintained alive in the foam, their movement can be controlled by illumination. Attractive, positive phototactic movement is observed in low intensities of the light flux contrary to high intensities, where repulsive, negative phototactic movement is observed.[16,17] When the *C. reinhardtii* cell is oriented parallel to the flux of light it reaches an average kinematic velocity of 100 μm s^{-1} in natural environments.[18] The wavelength of the light also alters the magnitude of photoadhesion observed in the *Chlamydomonas* species.[19]

The phototaxis tendency offers opportunities to perform controlled experiments related to algae dynamics. For instance, a very recent study discusses the algae retention in three dimensional foams using *Chlamydomonas reinhardtii* as the model algae.[20] This study was conducted in foams containing significantly larger bubbles compared to the present study, which allowed true three dimensional swimming of the algae within the Plateau borders. In that case the living algae favored the Plateau border corners. Therefore, as opposed to their non-swimming counterparts, they would not follow the liquid outflux, such as that caused by drainage.

Confinement influences the motion of microswimmers and fluid transport.[21] Walls and obstacles usually act as barriers guiding the swimming route. However, in certain situations they may also enhance the motility of the swimmers.[21–24] In the present study, we utilize the Plateau borders that in our quasi 2D setup create a channel with three walls: two liquid–air interfaces from neighboring bubbles and the covering plexiglass. These natural capillaries of the foam provide an excellent setting to study the movement of microswimmers under different confinements.

2 Methods

The experimental methods consist of three parts: (i) cultivating the algae and preparing the foam, (ii) the confinement apparatus with imaging and (iii) image analysis.

2.1 Cultivating the algae and preparing the foam

The algae used in the experiments represent a single-cellular phototactic micro-organism species known as *C. reinhardtii* of strain CC-125+, that belong to the group of green algae. The common diameter of the nearly spherical cells of this strain is $d = 10 \pm 2.5$ μm.[16,25,26] The size and shape of the cells vary between strains while the size is also affected by the individual lifetime between different growth phases. *C. reinhardtii* cells have two flagella that enable their motility by propulsion in a breaststroke fashion, and are also used for mating and feeding.[25] The rhodopsin-based proteins in the photoreceptors of the eyespot located on the side of the cell enables them to sense the light.[16,17] To scan the light from different directions, a *C. reinhardtii* cell rotates around its axis during the forward swimming with a rotation frequency of 0.2 to 2.0 Hz, which is insignificant compared to the beating frequency (25–60 Hz).[17,25,27] Fig. 2 shows a schematic as well as microscopic image of our microswimmer.

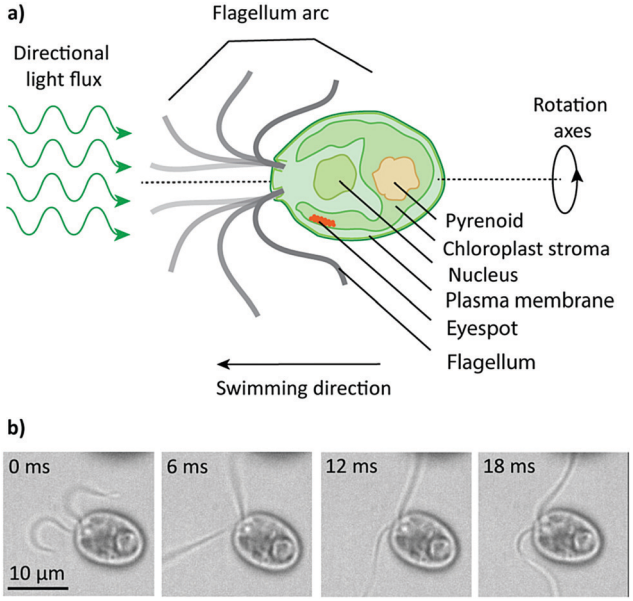

Fig. 2 (a) Schematic picture of a *C. reinhardtii* cell. (b) Microscopic images of a *C. reinhardtii* strain CC-125+ used in the experiments. The characteristic length of the algae is approximately equal to $d = 10$ μm. Images were taken on a Nikon Ti-E microscope,using a 60×/1.4 oil immersion objective lens, and an Andor Zyla sCMOS 5.5 camera.

C. reinhardtii used in the experiments were cultivated from stock wild type 137 and refined as CC-125 mt+ cultivars,[28] purchased from the *Chlamydomonas* Resource Center, University of Minnesota.[29] To enable proper cultivation, Sueoka high salt medium was created consisting of reagents described in Table 1.[30]

Original cultures were placed atop 1.5 wt% of agar agar gel (LB Agar Miller, Fisher Bioreagents BP1425-500) in HS medium

Table 1 The table presents all reagents and their respective amounts in high salt medium. Chemical quantities were measured with analytical scale (Mettler Toledo) with $\Delta m = 0.1$ mg display resolution. Beijerinck solution (HS Beij) and phosphate solution (HS Phos) were filled with Milli-Q water up to the desired concentration mentioned in the table

HS medium					
HS Beij (5 ml)		HS Phos (5 ml)		Other reagents	
Reagent	($g\ l^{-1}$)	Reagent	($g\ l^{-1}$)	Reagent	(ml)
NH_4Cl	100	K_2HPO_4	288	Milli-Q	985
$CaCl_2{\cdot}2H_2O$	2	KH_2PO_4	144	Hutner-sol	1
$MgSO_4{\cdot}7H_2O$	4	—	—	—	—

in sterile Petri dishes (Corning), which were sealed with parafilm (vwr PARAFILM) under aseptic conditions in a biosafety cabinet.

The active *C. reinhardtii* were cultured in 150 ml of high salt medium. The containers were connected to aeration tubing (Fisherbrand™ Silicon Platinum-cured Tubing 11502573, diameter 9 mm) equipped with sterile filters (Fisherbrand™ Sterile PES 15206869), to prevent harmful effects on cells due to excess oxygen during their photosynthesis. The evaporated water was replenished by connecting a bottle of Milli-Q water with an air pump, to keep the salt concentration constant.

The culturing setup was placed in an incubator (thermostatically controlled incubator, Lovibond), on top of a shaker (Grant-bio PSU-10i) which rotated with 100 rpm angular speed. The temperature inside the incubator was set to 27 °C. Periodic illumination was used to achieve a synchronized size culture. The light cycle consisted of 10 hours of illumination with a constant flux of 30 W m^{-2} cold white light, followed by 14 hours of darkness.

Cultures were renewed once every seven days by diluting in HS medium at a ratio of 1 : 1000, and stock populations in agar plates every third week. The number density of cells in the cultures used for experiments was around 10^6 cells per μl.

A surfactant solution, allowing a reproducible production of dry foam using the Tessari method,[31] was produced from saponin (Sigma-Aldrich 47036) for the experiment. The solution consisted of high salt medium, active *C. reinhardtii* cells and saponin (c = 0.5 g ml^{-1}).

In order to produce a microfoam, an advanced technique utilizing the original Tessari method was used.[32] Two horizontal syringes were placed in parallel with a single vertical syringe in order to minimize the average radius of the bubbles. 3.5 ml of solution was drawn into the vertical syringe and the two horizontal syringes were filled with air (10 ml in total). All syringes were pumped back-and-forth twenty times, after which the vertical syringe was attached to the Hele-Shaw chamber. The resulting foam in the quasi-2D chamber creates channels for the algae to swim in. This confinement is a Plateau border with a triangular shaped cross-section. Two of the walls are curved created by the neighboring bubbles and one wall is the plexiglass.

2.2 Confinement chamber and imaging

The complete geometry of the experimental setup is depicted in Fig. 3. The sealant between the plexiglass panels was made of waterproof tape. A thin Teflon ribbon (Scotch, Water Blocking Tape) was attached atop the sealant to prevent leaking and flow of material within the chamber during experiments. A hole was drilled on the side of the sealant and a needle (CHIRANA T. *Injecta*, Medoject) matching the hole size was inserted into the gap. Four additional holes were drilled on the opposite side of the chamber to even out the pressure.

The chamber was initially filled with foam stored in the vertical syringe. After pumping the syringe was removed from the needle, and the inlet was clogged with a Teflon ribbon. Experiments were recorded using a camera (Canon, EOS M3).

Five minutes of video recording at a 25 Hz frame rate was captured for each experiment. The lens system was built from a

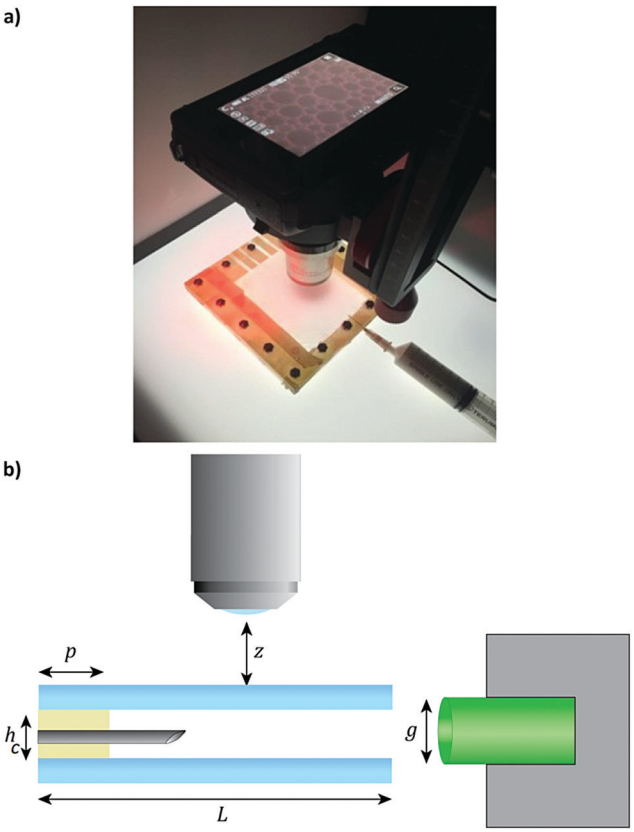

Fig. 3 Experimental setup with a square-like Hele-Shaw setup and a Canon EOS M3 camera. The chamber was built from two $L \times L$ = 100 × 100 mm plexiglass panels, and a sealant was laid in between. The attractive green light with an optical cable diameter of g = 1.2 mm is placed in the same horizontal lane as the injecting needle. The injecting needle is placed orthogonally to the flux of attractive light. In order to prevent the Hele-Shaw setup from leaking a h_c = 0.5 mm thick sealant with a width of p = 8.0 mm is used. In order to maximize the accuracy of the camera, the microscope lens was brought z = 1.0 mm close to the plexiglass of the Hele-Shaw setup.

microscope objective (2× 0.15 NA ultra Compact Object, EdmundOptics), to which a magnifying objective (20× Extension Tube, EdmundOptics) was attached.

The chamber was placed on top of a lighting pad with an illumination strength of 11.37 W m^{-2}. The background lighting was crucial for efficient operation of the particle detection Matlab scripts. A green light (12 W Twinkle RGBW LED Fiber Optic, CHINLY) was placed perpendicular to the needle to trigger positive phototactic responses and attract the active swimmers. The wavelength of light at full width half maximum is λ_w = 532.5 ± 32.5 nm.

2.3 Image analysis

The raw video was then interpolated to frames with 5 Hz. The image processing was executed using a custom Matlab script. The Color Thresholder app was utilized in the binary masking technique, in which a frame to be analyzed was segmented into the black and white parts of a user determined scale as illustrated in Fig. 4. As a result, the bulk liquid around targeted

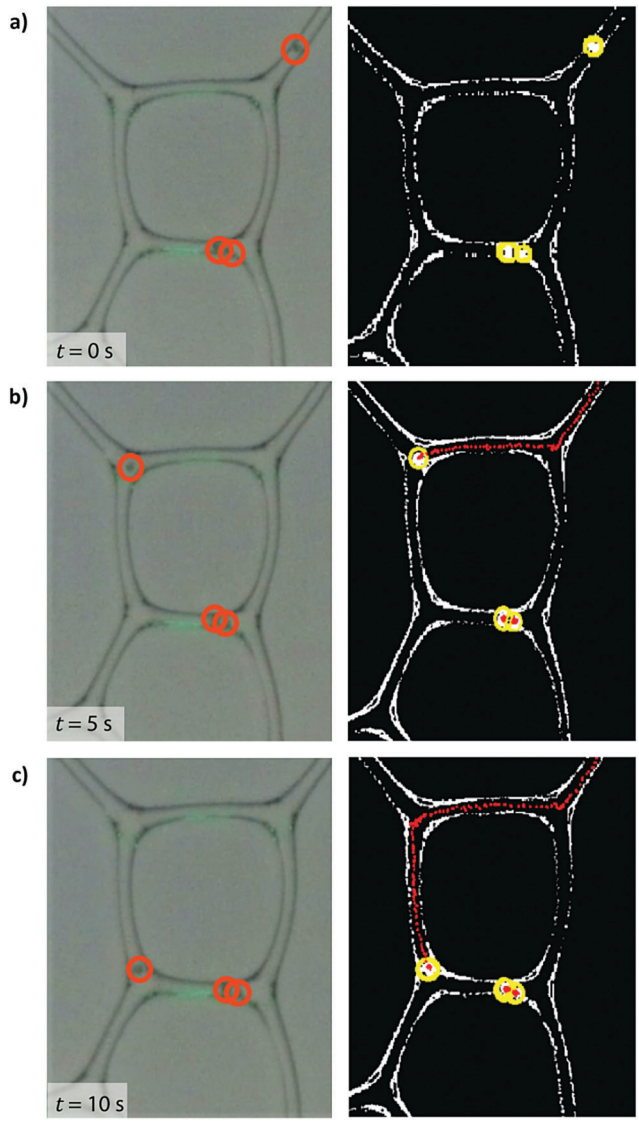

Fig. 4 The image series from (a)–(c) shows the original raw images (left) and binarized (right) images used in the analysis. The detected algae particles are highlighted by a red circle. One particle is moving and two that are entangled together. The time progresses as we go down the column from (a) t = 0 s to (c) t = 10 s. The binarized image shows the white edges of the bubble films that define the width h of the channel. The detected location of the alga is now highlighted with yellow and its measured path or previous locations are highlighted with red dots.

circular algae objects were tinted black. Consequently, the examined cell structure tinted white isolated the structure from surrounding elements. A Matlab function *Centers = imfindcircles*(A,r) based on the Hough transform was used in liaison with binary masking to locate circular cell objects with radius r in manipulated image A. The parameter $r = [r_{min}, r_{max}]$ contains the minimum radius value r_{min} and maximum radius value r_{max} of the accepted radii for the algae.

Radius value parameters r_{min} and r_{max} are confined within a pixel area of 45 to 65, which corresponds to the characteristic *C. reinhardtii* cell diameter. In this case, neither the surrounding bubbles nor minuscule particles were qualified as circles. As a result, a two-column matrix *centers* is obtained, which contains center point coordinates x, y for all circles regarding every particle perceived within the examined frame. The fundamental accuracy of binary masking is dependent on the isotropic background light intensity of the lighting pad.

The kinematic swimming velocity of an alga particle was measured by comparing values of *centers* matrix between each frames. The procedure was repeated for different channel widths h.

The channel width h was measured by lowering the radius parameter values to take into account smaller detectable white areas in the vicinity of previously observed algae particles. Opposing bubble wall circles were chosen and trajectories were drawn between pairs. Consequently, wall circle pairs with trajectories containing the examined algae particle center coordinates were chosen. Pairwise distances were calculated and the average value h_{frame} for each frame was calculated. Furthermore, frame-wise values were averaged to calculate the final channel width h for the previously measured kinematic velocity value of the algae particles.

Due to the quasi 2D nature of the environment illustrated in Fig. 5, the channel width h is converted into an effective channel width or confinement parameter:

$$\lambda = \frac{h}{\cos\alpha}, \tag{1}$$

where $\alpha = 45^\circ$ is the angle of the liquid–air interface that is seen as a dark line in our camera. Fig. 5 is a schematic of the cross-section of the fluid film (blue) near the plexiglass (gray). The orange circle with radius λ then describes the radius of the cylindrical confinement. Here, we would like to emphasize that we measure h and convert it into the effective channel width λ. Both are characteristic length scales that represent the space where the algae can swim. In the following section we use both: h is used when presenting the raw data and λ when interpreting the model.

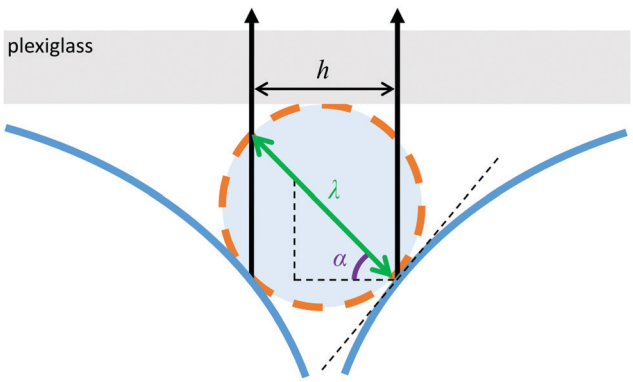

Fig. 5 The cross-section of the quasi 2D fluid–air interface (large blue arcs) has a curvature near the top plexiglass. The space where the alga swims can be then approximated as a cylindrical confinement. The orange circle depicts the cross-section of this confinement with diameter λ (green). The observed channel boundaries (black vertical arrows) with separation h are interference patterns of reflected light at an angle α = 45° from the liquid–air boundary defining the size of the confinement.

3 Results

Next, we show the movement of the algae observed directly from the images, measured using the algorithm detailed in Section 2.3 and propose a simple force balance model describing the motion of the algae.

Fig. 6 shows the raw measurement data: the algae motion for different channel widths h. Here, the image is enhanced for clarity by cropping a single film and enhancing its contrast. The right column represents a time series for algae swimming in a wide channel. The algae do not touch the wall and we observe speeds similar to the bulk flow. In contrast, the left column shows the motion when the width of the channel is extremely narrow. The body of the alga touches the borders of the confinement and the alga is forced to drag itself along the walls. From these cases we conclude that there are two limits as expected: bulk limit and wall drag limit. Next, we check that this movement is originated from the swimming algae and not *e.g.* fluid motion.

In most cases, positive phototactic swimming was observed. As the green attractive light was placed perpendicular to the arrival trajectory of active matter in the start of the experiment, the majority of the observed algae cells were observed to steer towards the attractive light. The steering towards light was most evident in multiply connected nodes. In these nodes, where larger volume was available, the alga was able to rotate its structure accordingly to allow its movement towards the attractive light flux. Thus it can be concluded that algae can be guided through the bubble labyrinth using attractive lighting.

The flow of liquid within foam channels was minimal. This phenomenon was distinguishable due to the presence of tiny algae-sized bubbles co-floating with the algae within the channel geometry. However, it was noticed that the stray movement of these bubbles was very small compared to the active movement speed of the algae particles. In every conducted experiment, the possible flow velocity of said tiny bubble particles was surpassed by algae particles present in the same regions. In addition, the scarce occasional coarsening of the foam was noted to have little effect on the motion of particles. In addition, we performed additional control experiments with polymer and polystyrene carboxylate microparticles with d = 10 μm diameter. We found that most of the particles remained stationary, thus indicating no fluid motion or particle pinning. The ones that move due to diminutive flows do so at very low speeds compared to the algae movement. Near a T2 event, where a bubble vanishes due to foam coarsening, the immobile particle was found to achieve a temporary top velocity of v_p = 2 μm s^{-1}. Even in this extreme case scenario, the particle motion is significantly smaller than the swimming of the algae and later we can observe that the fluctuation between the different measurements are much larger. Hence, we can conclude that the fluid motion in the Plateau borders can be neglected.

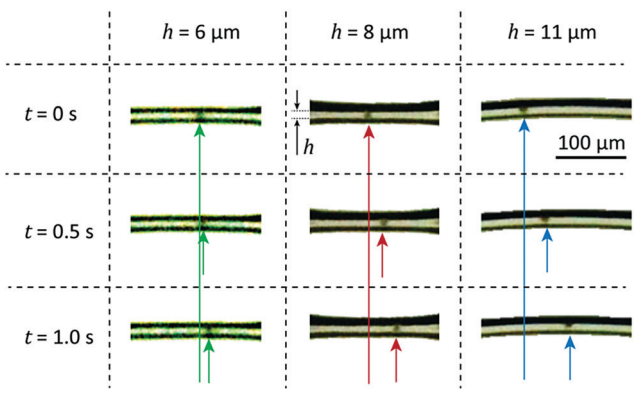

Fig. 6 Stacked image shows the movement of algae for various liquid film widths. As the film thickness reaches the wall drag limit, bubble walls begin to exhibit frictional forces affecting algae movement. This results in the reduction of net propulsive forces generated by flagellar strokes.

For very wet foams with low gas fraction (*e.g.* in Fig. 1) the channel width is much larger than the algae width. In these foams, where the effective channel width is $\lambda > 10$ μm, the average velocity value of $v_{max} = 100 \pm 5$ μm s^{-1} was observed. This result matches the velocity values discovered in previous experiments.[18,26] Consequently, *C. reinhardtii* cells were observed to execute positive phototactic movement towards the attractive light. The wall drag limit was reached when the effective film width λ was narrowed to below 10 μm down to approximately the characteristic diameter d of *C. reinhardtii* algae cells. As the effective bubble film width λ reached the wall drag limit, algae swimming speed began to reduce drastically due to the increased interactions between the body of the algae and the walls of the confinement as illustrated in Fig. 6. The reduction in motility can be estimated to originate from the contact forces between the bubble walls and the cell structure. As a result, the normal circulation of algae flagella strokes was hindered lowering the overall velocity v of the cell object.

Fig. 7a shows the velocity v for various channel widths. The data show clearly three different cases. The blue circles represent the cases where the body of the alga is touching the bubble wall causing elastic deformation to the surfactant layer and the system is overdamped. The alga drags itself through the channel and a part of the energy goes to the deformation of the bubble walls. The green triangles represent the bulk case, where the alga swims at its maximum speed. The films are merely guiding the alga, but not restricting its motion. In between the unlimited bulk and overdamped drag cases there is an intermediate region shown by red squares. The motion is somewhat restricted in a linear fashion. We hypothesize that at this regime the shear rate of the liquid layer between the alga and the walls of the confinement plays a significant role. Based on the simplified assumption that there is an effective gap of fluid, we can construct a simple force balance equation to explain the linear slope between the two extreme cases.

To further scrutinize the shear dominated regime, limiting our considerations to viscous dissipation, we can write an expression for the driving force generated by the algae F as

$$F = \eta \dot{\gamma} A, \quad (2)$$

where η = 1 mPa s is the viscosity of the liquid layer (containing low concentrations of saponin used as the foaming agent), A is the side area of the alga particle and $\dot{\gamma}$ is the shear rate caused

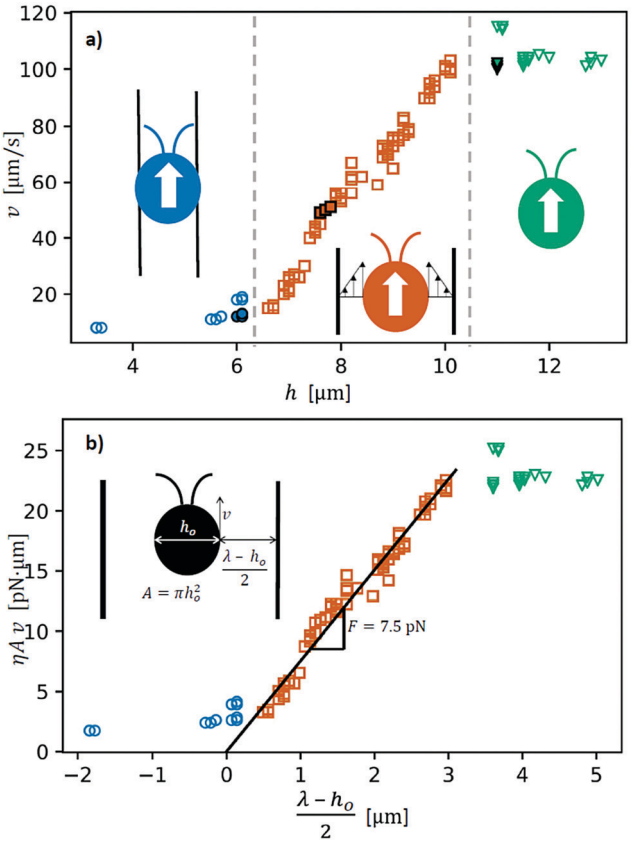

Fig. 7 (a) Raw data measured by the image analysis scripts in Matlab. Kinematic velocities v of individual cells are related to raw, measured channel widths h. The data split into three regions indicated by the color coding: (i) alga body is touching the wall (blue circles) (ii) high shear rate between the alga and the wall (red squares) and (iii) unconstricted swimming (green triangles). The filled symbols are the same data as in Fig. 6. (b) Data are presented to match the analytical expression by scaling the data using the material parameters. The slope now gives the force needed to propagate in the bubble films. Here, we use the effective channel width λ.

by the movement of the algae body with respect to the bubble film. The viscosity η is confirmed in an auxiliary experiment with a shear rate range $\dot{\gamma} = 0.1$–$100\ s^{-1}$ using the Anton Paar 302 rheometer.

Here, we simplify the geometry by approximating the alga as a spherical object with a side area of total $A = \pi h_o^2\ \mu m^2$ where h_o is the diameter shown in the inset of Fig. 7b. Also, the channel is approximated as a cylindrical tube of diameter λ corresponding to measured gap h in the images (Fig. 6) *via* eqn (1). Finally, we assume that the alga velocity goes to zero $v = 0\ \mu m\ s^{-1}$ when the alga body diameter h_o equals the effective channel diameter $h_o = \lambda_{v=0} = 8.3\ \mu m$ and the alga body begins to touch the walls of the confinement shown in Fig. 7a. Putting the ingredients together we get a relation between the velocity of the alga v and channel width:

$$\eta A v = F(\lambda - h_o)/2. \quad (3)$$

The slope of fit in the Fig. 7b is then the effective driving force of the algae $F = 7.5$ pN. In such a simple model we are neglecting the effects of fluid backflow, observed to increase the drag coefficient in the sedimentation of passive particles confined by slipping boundaries.[33] Despite this, the fitted dimensions are at the same ballpark as the literature values for algae of $d = 10 \pm 2.5\ \mu m$, which is roughly the size of the algae in the present experiments, as confirmed by our high magnification microscope image (Fig. 2). Also the literature values for forces measured using various methods range between 5 and 50 pN.[34,35] We may only speculate that here the drag coefficient might be compensated, for instance, by the solid–liquid boundary conditions at the algae–liquid interface, which may differ from those for passive particles. Furthermore, we wish to emphasize that the above considerations do not take into account the possible film–flagella interactions that may either enhance or weaken the propulsion generated by the algae. Therefore, the propulsion forces computed above should be taken with caution.

Fig. 8 shows the standard deviation of velocity σ_v for different channel widths obtained from the v *vs.* h data for each of the regions of Fig. 7, overdamped (blue circles), transition (red squares) and bulk (green triangles) regions. Each symbol represents the standard deviation of the velocities in a window around $v(h)$, $[h - 1.5\ \mu m;\ h + 1.5\ \mu m]$ to compensate for the quantity of data. The high standard deviation in the transition region indicates that the alga occasionally interacts with the walls of the confinement. This result is expected as the geometry reduces the spiral motion of the algae as the flagella have only two planes in which they can move, parallel to the plexiglass or parallel to the bubble film. This constraint leads to a motion where the alga, or its flagella is bound to hit the plexiglass or the bubble walls multiple times creating intermittent movement. In particular, in narrow channels the interaction between the flagella and borders of the confinement leads to a complex behavior such as the centering of the swimmer as in the case of helical microswimmers.[36] In future modeling this should be taken into consideration.

To summarise, our simple ball-in-tube approximation thus works surprisingly well. At this point, we see no need for further

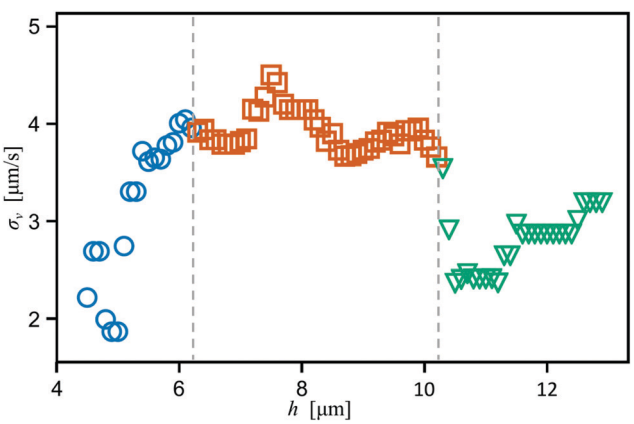

Fig. 8 Standard deviation of the algae velocity is larger in the transition region (red squares) than in the overdamped (blue circles) or bulk (green triangles) region. This indicates that the motion in the transition region is not smooth as the alga occasionally interacts with the walls of the confinement.

fine tuning as our focus lies on the interaction between the algae and the bubbles. We can observe the movement of the algae in much narrower channels than the body width of the algae and thus conclude that the algae in fact are exerting forces to deform the films.

4 Conclusions

We have performed novel experiments showing that it is possible to create a foam like environment for the algae to live in and furthermore control the speed and direction of the algae. The algae *Chlamydomonas reinhardtii* as self-propelled particles managed to execute precise navigation in a network of bubble films as we have shown in Fig. 7. Self-direction of the individual active cells was affected by utilization of attractive external light stimulus, thus turning the entire algae population residing inside the Hele-Shaw cell into a moving host of controllable biomass. The movement of algae swimmers can be measured and predicted by using tuned Matlab scripts and a knowledge of the foam structure.

We show that an alga swimmer has two limiting factors of its movement speed. The lower limit emerges from the overdamped dynamics where the body of the algae touches the walls of the confinement. The upper limit is due to the balance between the drag force caused by the surrounding fluid and the maximum propulsion force produced by the algae. In the region between these two, the films hinder the optimal swimming of the algae. There, the reduction of the algae swimming speed is explained by our simplified model where the shear rate between the body of the algae and bubble film increases as the channel becomes narrower *i.e.* the drag force increases linearly due to the finite size of the channel. In addition, alteration of the algae movement caused by coincidental regional coarsening of the foam was observed to be minimal.

Earlier research reports non-linear dependence of the drag with respect to the particle size–channel width ratio in the channels with slip boundary conditions at the channel walls.[33] This is assigned to the backflow introduced by the fluid volume conservation due to the motion of the particle. Here we did not observe the same behavior for active particles. This might be because of (i) the occurrence of the backflow outside the Plateau borders, (ii) effects such as boundary–flagella interactions[37] that may influence the swimming efficiency of the algae or (iii) the hydrodynamics of the particle–liquid interface, which may be very different for passive particles and algae. Any (or all) of these might then compensate for the backflow effect causing a linear dependence of the velocity in the transition regime. Therefore, this clearly suggests further detailed future studies on the swimming of algae in contact with surfactant covered deformable walls.

One application area of an algae–foam system is in the field of novel bioreactors, where algae like swimmers produce or transport *e.g.* components for the medical industry. Their food, nutrients and gases as well as collection of the end product can be controlled by continuous flow of foam, and in this case, light.

From the fundamental physics perspective at higher number densities of the algae particles, the foam as a complex fluid can be expected to be manipulated by the local noise provided by the algae. This can be anticipated to lead to a spontaneous local yield in such active foam systems. Thus, we have now successfully created a template, which possibly allows us to prepare active foam, a foam that contains controllable active particles that in the future can be used to study the effect of small scale disorder on the macroscopic properties of the foam.

Conflicts of interest

There are no conflicts to declare.

Acknowledgements

J. K., A. P. and J. V. I. T. acknowledge the funding from the Academy of Finland (308235, 278367 and 316219) and Aalto University (974109903) as well as the Aalto Science IT project for computational resources.

Notes and references

1 A. T. Brown, I. D. Vladescu, A. Dawson, T. Vissers, J. Schwarz-Linek, J. S. Lintuvuori and W. C. Poon, *Soft Matter*, 2016, **12**, 131–140.
2 V. J. Langlois, *J. Rheol.*, 2014, **58**, 799–818.
3 R. Jeanneret, D. O. Pushkin and M. Polin, *Phys. Rev. Lett.*, 2019, **123**, 248102.
4 N. Ueki and K.-i. Wakabayashi, *Bio-Protoc.*, 2017, **7**, e2356.
5 D. L. Weaire and S. Hutzler, *The Physics of Foams*, Oxford University Press, 2001.
6 A. Janoska, P. P. Lamers, A. Hamhuis, Y. van Eimeren, R. H. Wijffels and M. Janssen, *Chem. Eng. J.*, 2017, **313**, 1206–1214.
7 C. Brennen and H. Winet, *Annu. Rev. Fluid Mech.*, 1977, **9**, 339–398.
8 E. M. Purcell, *Am. J. Phys.*, 1977, **45**, 3–11.
9 J. Elgeti, R. G. Winkler and G. Gompper, *Rep. Prog. Phys.*, 2015, **78**, 056601.
10 J. Adler, *Science*, 1966, **153**, 708–716.
11 M. G. Petrino and R. Doetsch, *Microbiology*, 1978, **109**, 113–117.
12 B. Liebchen, P. Monderkamp, B. ten Hagen and H. Löwen, *Phys. Rev. Lett.*, 2018, **120**, 208002.
13 C. Dieckmann and T. Mittelmeier, *eLife*, 2016, **5**, e14169.
14 R. L. Stavis and R. Hirschberg, *J. Cell Biol.*, 1973, **59**, 367–377.
15 R. Jeanneret, M. Contino and M. Polin, *Eur. Phys. J.: Spec. Top.*, 2016, **225**, 2141–2156.
16 P. Hegemann, *Annu. Rev. Plant Biol.*, 2008, **59**, 167–189.
17 R. R. Bennett and R. Golestanian, *J. R. Soc., Interface*, 2015, **12**, 20141164.
18 X. Chen, L. Zeng, Y. Wu, Y. Gao and Y. Zhao, *Energy, Ecol. Environ.*, 2017, **2**, 289–295.
19 C. T. Kreis, M. Le Blay, C. Linne, M. M. Makowski and O. Bäumchen, *Nat. Phys.*, 2018, **14**, 45–49.
20 Q. Roveillo, J. Dervaux, Y. Wang, F. Rouyer, D. Zanchi, L. Seuront and F. Elias, *J. R. Soc., Interface*, 2020, **17**, 20200077.
21 E. Lauga and T. R. Powers, *Rep. Prog. Phys.*, 2009, **72**, 096601.

22 R. Ledesma-Aguilar and J. M. Yeomans, *Phys. Rev. Lett.*, 2013, **111**, 138101.
23 M. Theers, E. Westphal, G. Gompper and R. G. Winkler, *Soft Matter*, 2016, **12**, 7372–7385.
24 V. Magdanz, B. Koch, S. Sanchez and O. G. Schmidt, *Small*, 2015, **11**, 781–785.
25 J. K. Hoober, *Science*, 1989, **246**, 1503–1505.
26 X. Garcia, S. Rafa and P. Peyla, *Phys. Rev. Lett.*, 2013, **110**, 138106.
27 J. S. Guasto, K. A. Johnson and J. P. Gollub, *Phys. Rev. Lett.*, 2010, **105**, 168102.
28 T. Pröschold, E. H. Harris and A. W. Coleman, *Genetics*, 2005, **170**, 1601–1610.
29 *The Biological Resources of Model Organisms*, ed. R. L. Jarret and K. McCluskey, CRC Press, Boca Raton, 2019.
30 N. Sueoka, *Proc. Natl. Acad. Sci. U. S. A.*, 1960, **46**, 83–91.
31 L. Tessari, A. Cavezzi and A. Frullini, *Dermatol. Surg.*, 2001, **27**, 58–60.
32 J. Xu, Y.-F. Wang, A.-W. Chen, T. Wang and S.-H. Liu, *SpringerPlus*, 2016, **5**, 129.
33 O. Pitois, C. Fritz, L. Pasol and M. Vignes-Adler, *Phys. Fluids*, 2009, **21**, 103304.
34 T. J. Böddeker, S. Karpitschka, C. T. Kreis, Q. Magdelaine and O. Bäumchen, *J. R. Soc., Interface*, 2020, **17**, 20190580.
35 R. P. McCord, J. N. Yukich and K. K. Bernd, *Cell Motil. Cytoskeleton*, 2005, **61**, 137–144.
36 J. LaGrone, R. Cortez and L. Fauci, *Phys. Rev. Fluids*, 2019, **4**, 033102.
37 C. T. Kreis, A. Grangier and O. Bäumchen, *Soft Matter*, 2019, **15**, 3027–3035.

